

# OMG-Agent: Toward Robust Missing Modality Generation with Decoupled Coarse-to-Fine Agentic Workflows

Ruiting Dai<sup>1</sup>, Zheyu Wang<sup>1</sup>, Haoyu Yang<sup>1</sup>, Yihan Liu<sup>1</sup>, Chengzhi Wang<sup>1</sup>, Zekun Zhang<sup>1</sup>, Zishan Huang<sup>1</sup>, Jiaman Cen<sup>1</sup> and Lisi Mo<sup>1</sup>

<sup>1</sup>University of Electronic Science and Technology of China  
weldaspica@gmail.com

## Abstract

Data incompleteness severely impedes the reliability of multimodal systems. Existing reconstruction methods face distinct bottlenecks: conventional parametric/generative models are prone to hallucinations due to over-reliance on internal memory, while retrieval-augmented frameworks struggle with retrieval rigidity. Critically, these end-to-end architectures are fundamentally constrained by Semantic-Detail Entanglement—a structural conflict between logical reasoning and signal synthesis that compromises fidelity. In this paper, we present **Omni-Modality Generation Agent (OMG-Agent)**, a novel framework that shifts the paradigm from static mapping to a dynamic coarse-to-fine Agentic Workflow. By mimicking a *deliberate-then-act* cognitive process, OMG-Agent explicitly decouples the task into three synergistic stages: (1) an MLLM-driven Semantic Planner that resolves input ambiguity via Progressive Contextual Reasoning, creating a deterministic structured semantic plan; (2) a non-parametric Evidence Retriever that grounds abstract semantics in external knowledge; and (3) a Retrieval-Injected Executor that utilizes retrieved evidence as flexible feature prompts to overcome rigidity and synthesize high-fidelity details. Extensive experiments on multiple benchmarks demonstrate that OMG-Agent consistently surpasses state-of-the-art methods, maintaining robustness under extreme missingness, e.g., a 2.6-point gain on CMU-MOSI at 70% missing rates. The source code is available at <https://anonymous.4open.science/status/OMGAgent-8HSN>.

## 1 Introduction

Multimodal Large Language Models (MLLMs) [Xu *et al.*, 2025; Ye *et al.*, 2023] have redefined machine perception and generation across diverse tasks [Liu *et al.*, 2023]. However, their robustness is severely compromised by data incompleteness, where real-world inputs frequently lack essential modalities (e.g., video without audio) [Ma *et al.*, 2021]. Consequently, Missing Modality Reconstruction—the inference

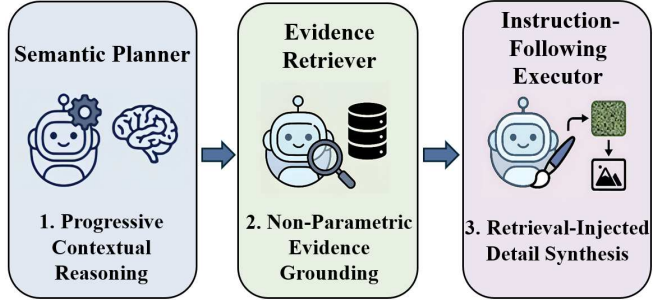


Figure 1: **Overview of OMG-Agent:** 1) Planner, 2) Retriever and 3) Executor. Three agents synergistically decouple high-level reasoning from low-level synthesis via a coarse-to-fine workflow.

and synthesis of missing components from partial observations—remains a critical bottleneck for reliable multimodal systems [Wu *et al.*, 2024].

Existing modality reconstruction methods have evolved alongside advances in generative paradigms. Early parametric models (e.g., GANs [Kang *et al.*, 2023], VAEs [Palumbo *et al.*, 2023]) relied on direct cross-modal mapping, often resulting in *parametric hallucination* due to an over-reliance on statistical correlations. The subsequent integration of generative MLLMs [Xu *et al.*, 2025] provided auxiliary contextual guidance, yet their utility is limited by an inherent propensity for *factual hallucination* [Zhang *et al.*, 2025]. More recently, Retrieval-Augmented Generation (RAG) frameworks have enabled grounded synthesis but inherently suffer from *retrieval rigidity*, where static databases fail to adapt to novel, compositional scenarios unseen in training data [Asai *et al.*, 2024].

More critically, these models [Liu *et al.*, 2025] mostly jointly optimize high-level semantic reasoning (deciding *what content to generate*) and low-level feature synthesis (deciding *how to generate details*) within a coupled end-to-end process. Due to the inherent one-to-many ambiguity of cross-modal mapping—where one semantic concept corresponds to a *manifold* of potential details—this coupling forces shared parameters to reconcile conflicting gradients, leading to an optimization dilemma that sacrifices semantic logic for detail fidelity, and vice versa. We term this phenomenon Semantic-Detail Entanglement, where gradient interference between abstract semantic alignment and low-level feature fitting impedes clear decision-making. This bottleneck compels us to address a

fundamental research question: *How can high-level semantic planning be decoupled from low-level detail synthesis to achieve verifiable and robust modality reconstruction?*

Inspired by the robust planning and tool-use capabilities of LLM-based Agents [Yao *et al.*, 2022; Schick *et al.*, 2023], we reformulate missing modality reconstruction from a static mapping problem into a dynamic Agentic Workflow, transcending traditional single-step reactive approaches [Rombach *et al.*, 2022]. This paradigm mimics a *deliberate-then-act* cognitive process, explicitly decomposing the entangled reconstruction process into three verifiable stages: contextual reasoning to infer missing semantics (Planning), active retrieval to ground these semantics in concrete evidence (Tool Use), and conditional generation to synthesize final details (Execution), as illustrated in Figure 1.

To realize this workflow, we propose the **Omni-Modality Generation Agent (OMG-Agent)**, a novel framework structured as a synergistic *Planner-Retriever-Executor* system. Specifically, an MLLM-driven Semantic Planner substantially mitigates input ambiguity via Progressive Contextual Reasoning, producing a structured semantic plan. Subsequently, an Evidence Retriever actively retrieves non-parametric feature anchors from external knowledge bases. Finally, an Instruction-Following Executor, which is instantiated as a retrieval-injected diffusion model, synthesizes high-fidelity details strictly aligned with the semantic plan and retrieved evidence.

The contributions of this paper are summarized as follows:

- We propose **OMG-Agent**, a novel framework that pioneers the reformulation of missing modality reconstruction as a coarse-to-fine Agentic Workflow, effectively resolving the Semantic-Detail Entanglement dilemma by decoupling high-level reasoning from low-level synthesis.
- We design an MLLM-driven Semantic Planner incorporating a Progressive Contextual Reasoning mechanism to substantially mitigate one-to-many mapping ambiguity by explicitly constraining the uncertain generation space into a structured semantic plan.
- We introduce a Retrieval-Injected Executor that synergizes with a non-parametric Evidence Retriever, effectively overcoming retrieval rigidity by utilizing external evidence as flexible feature prompts rather than fixed pixel templates to guide high-fidelity synthesis.
- Extensive experiments on multiple Datasets demonstrate consistent improvements over strong baselines across diverse missing patterns, maintaining robustness even at missing rates up to 70%, e.g., with 2.6 points improvement over the SOTA model.

## 2 Related Work

### 2.1 Multimodal Missing Modality Reconstruction

Missing modality reconstruction has been extensively studied in multimodal learning, where the goal is to infer and synthesize unobserved modalities from partial observations. Early approaches[Zhang *et al.*, 2024; Sutter *et al.*, 2024] primarily

rely on end-to-end parametric models that directly map observed modalities to missing ones, often leading to parametric hallucination due to their reliance on statistical correlations rather than deep semantic understanding. More recent methods introduce large language models as auxiliary components to provide contextual guidance[Nguyen *et al.*, 2025; Zang *et al.*, 2025], while Retrieval-Augmented Generation Diffusion frameworks [Sharma *et al.*, 2025; Song *et al.*, 2025] further ground generation with external samples. Despite these advances, these retrieval-augmented approaches inherently suffer from retrieval rigidity, as their dependence on finite, static databases limits semantic adaptability and hinders robust generalization to novel or compositional missing-modality scenarios.

## 2.2 Retrieval-Augmented Generation

Despite the success of retrieval-augmented generation in improving realism and grounding, existing methods typically entangle high-level semantic inference with low-level signal synthesis within a monolithic end-to-end pipeline. Given the inherent one-to-many ambiguity of cross-modal mapping, this coupling forces shared parameters to simultaneously decide what to generate and how to generate it, often resulting in conflicting optimization objectives. We refer to this structural limitation as semantic–signal entanglement, where implicit statistical matching dominates decision-making and hinders robust semantic planning[Huang *et al.*, 2025; Fan *et al.*, 2025]. This bottleneck underscores the necessity of explicitly decoupling high-level semantic planning from low-level signal synthesis in order to enable verifiable and robust modality reconstruction.

## 2.3 LLM Agents for Planning and Tool Use

LLM-based agents have recently demonstrated strong capabilities in explicit semantic planning, tool use, and multi-step decision-making through intermediate reasoning [Rawat *et al.*, 2025; Gao *et al.*, 2025]. By decomposing complex tasks into structured workflows, agentic systems enable deliberate planning and verifiable execution rather than single-step reactive generation. These characteristics closely align with the intrinsic requirements of multimodal generation and missing modality reconstruction, where high-level semantic decisions must be resolved prior to low-level signal synthesis. Accordingly, adopting an agent-based workflow provides a natural mechanism to decouple high-level semantic planning from low-level signal generation, effectively addressing the semantic–signal entanglement identified above and aligning with the reformulation proposed in this work.

## 3 Method

### 3.1 Problem Definition

We consider a multimodal sample  $\mathbf{x} = \{x^{(1)}, \dots, x^{(M)}\}$  with availability mask  $\mathbf{m} \in \{0, 1\}^M$ . This partitions the indices into an observed set  $\mathcal{O} = \{m \mid m^{(m)} = 1\}$  and a missing set  $\bar{\mathcal{O}} = \{1, \dots, M\} \setminus \mathcal{O}$ , yielding the observation  $X = \{x^{(m)} : m \in \mathcal{O}\}$  and the missing target  $Y = x^{(t)} (t \in \bar{\mathcal{O}})$ .

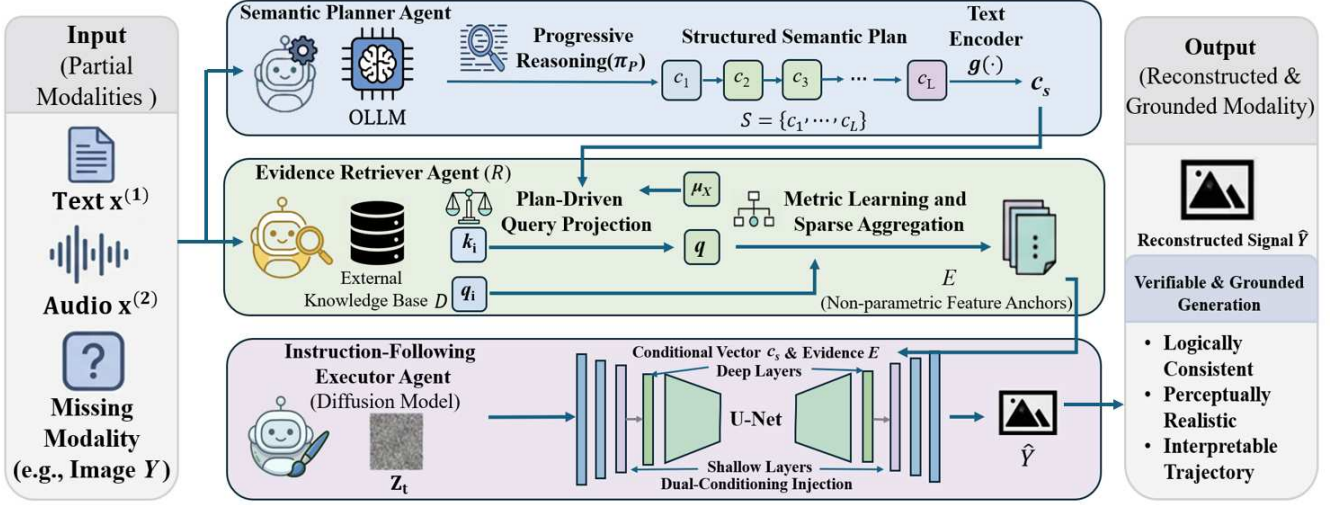


Figure 2: OMG-Agent Architecture. The workflow decouples generation into: (1) Semantic Planning:  $\pi_P$  reasoning for plan  $S$ ; (2) Evidence Retrieval:  $\pi_R$  anchoring  $S$  into evidence  $E$  from  $\mathcal{D}$ ; (3) Retrieval-Injected Execution:  $\pi_E$  synthesizing  $\hat{Y}$  via dual-conditioning of  $c_S$  and  $E$ .

To address the Semantic–Signal Entanglement inherent in static mappings  $\hat{Y} = f_\theta(X)$ , we reformulate the reconstruction task as generating an agentic cognitive trajectory. OMG-Agent produces a composite trajectory comprised of Planning–Retrieval–Execution:

$$\tau \triangleq (S, \mathcal{N}_K, E, \{z_T \rightarrow \dots \rightarrow z_0\}, \hat{Y}), \quad (1)$$

where  $S$  is the structured semantic plan (logical guidance),  $\mathcal{N}_K$  is the set of retrieved evidence indices (reference source),  $E$  is the aggregated non-parametric evidence (concrete anchor),  $\{z_T \rightarrow \dots \rightarrow z_0\}$  is the progressive denoising action sequence (dynamic process), and  $\hat{Y}$  is the final reconstruction.

We define optimal reconstruction as finding the trajectory  $\tau^*$  that maximizes a holistic Trajectory Utility, harmonizing the reasoning process with the synthesis result:

$$\tau^* = \arg \max_{\tau} \mathcal{U}(\tau; X, Y), \quad (2)$$

$$\mathcal{U}(\tau; X, Y) = -\mathcal{L}_{\text{rec}}(\hat{Y}, Y) - \lambda_s \mathcal{C}_{\text{sem}}(S, X) - \lambda_e \mathcal{C}_{\text{evi}}(S, E) - \lambda_p \mathcal{C}_{\text{path}}(\{z_t\}). \quad (3)$$

Here,  $\mathcal{L}_{\text{rec}}$  ensures synthesis fidelity, while  $\mathcal{C}_{\text{sem}}$  and  $\mathcal{C}_{\text{evi}}$  measure the logical consistency and alignment of the intermediate variables  $S$  and  $E$ , respectively.  $\mathcal{C}_{\text{path}}$  imposes regularization on the execution path, and  $\lambda_s, \lambda_e, \lambda_p$  are hyperparameters balancing these objectives.

## 3.2 OMG-Agent Overview

As depicted in Figure 2, OMG-Agent orchestrates a synergistic collaboration among three decoupled modules: the Semantic Planner ( $\mathcal{P}$ ), the Evidence Retriever ( $\mathcal{R}$ ), and the Instruction-Following Executor ( $\mathcal{E}$ ). Formally, we cast the inference as a sequential composition of policies:  $S = \pi_P(X)$ ,  $(E, \mathcal{N}_K) = \pi_R(X, S; \mathcal{D})$ , and  $\hat{Y} = \pi_E(X, S, E; \xi)$ , where  $\mathcal{D} = \{d_i\}_{i=1}^N$  represents an external multimodal knowledge base of semantic-feature pairs, and  $\xi \sim \mathcal{N}(0, \mathbf{I})$  denotes the stochastic noise for diffusion sampling. This explicit decomposition fosters a

transparent and verifiable reasoning trajectory: the Planner  $\pi_P$  functions as the reasoning engine to disentangle ambiguous observations  $X$  into a deterministic logical structure  $S$ ; the Retriever  $\pi_R$  serves as the grounding tool to actively anchor this logic into concrete evidence  $E$  from  $\mathcal{D}$ ; and the Executor  $\pi_E$  operates as the synthesis engine to generate the final signal  $\hat{Y}$  under dual constraints.

## 3.3 Semantic Planner ( $\mathcal{P}$ ): Progressive Reasoning for Plan Generation

The goal of the Semantic Planner ( $\mathcal{P}$ ) is to clarify the semantic constraints that the missing modality must satisfy before execution. This corresponds to the Planning phase in the trajectory  $\tau$ . By establishing a unified logical skeleton, this module effectively reduces the uncertainty inherent in cross-modal one-to-many mappings.

**Progressive Reasoning and Canonical Representation.** We employ an LLM-based policy  $\pi_P$  to perform multi-step reasoning. The generation of the  $\ell$ -th constraint follows an autoregressive chain conditioned on the observation  $X$  and preceding constraints:  $c_\ell \sim \pi_P(\cdot | X, c_{<\ell})$ . The resulting plan  $S \triangleq \{c_1, \dots, c_L\}$  is a sequence of discrete semantic constraints adhering to the pre-defined Schema (a template format ensuring executability). To facilitate downstream processing, we introduce a pre-trained text encoder  $g(\cdot)$  from Omni-LLM to map the discrete plan into a continuous condition vector:

$$c_S = g(S) \in \mathbb{R}^{d_S}. \quad (4)$$

**Candidate Re-ranking via Constrained Maximization.** To improve plan quality, we sample a candidate set  $\Omega(X)$  and select the optimal plan  $S^*$  by maximizing a regularized scoring objective:

$$S^* = \arg \max_{S \in \Omega(X)} \left\{ \sum_{\ell=1}^L \log \pi_P(c_\ell | X, c_{<\ell}) - \lambda_s \mathcal{C}_{\text{sem}}(S, X) - \gamma \mathbb{I}_{\text{schema}}(S) \right\}. \quad (5)$$

where the first term represents the reasoning confidence;  $\lambda_s$  and  $\gamma$  are balancing hyperparameters; and  $\mathbb{I}_{\text{schema}}(S)$  is an indicator penalty function (equaling  $\infty$  if  $S$  violates the Schema format, and 0 otherwise). Finally,  $\mathcal{C}_{\text{sem}}$  denotes the **semantic consistency cost**, penalizing plans that deviate from the input context:

$$\mathcal{C}_{\text{sem}}(S, X) = 1 - \frac{g(S)^\top \psi(X)}{\|g(S)\| \|\psi(X)\|}, \quad (6)$$

where  $\psi(\cdot)$  is the pre-trained multimodal encoder from Omni-LLM aligned with  $g(\cdot)$  to extract observation features. This term ensures high-fidelity alignment between the logical structure and the observation in the shared semantic space.

### 3.4 Evidence Retriever ( $\mathcal{R}$ ): Acquiring Traceable Evidence

The core mission of the Evidence Retriever ( $\mathcal{R}$ ) is to **ground** the abstract semantic plan  $S$  into the external knowledge base  $\mathcal{D} = \{d_i\}_{i=1}^N$ , returning a traceable evidence chain  $(\mathcal{N}_K, E)$ . This corresponds to the Retrieval phase in the trajectory  $\tau$ . By utilizing non-parametric external evidence as flexible feature prompts rather than fixed pixel templates, this module guides high-fidelity synthesis while mitigating detail fabrication caused by reliance on purely parametric memory.

**Plan-Driven Query Projection.** To ensure the retrieval process considers both input similarity and strictly adheres to the planned intent, we construct a composite query vector  $q$ . Specifically, we fuse the observation embedding  $u_X$  with the plan condition  $c_S$  via feature concatenation and map them through a learnable projection network:

$$q = \sigma(W_q[u_X \oplus c_S] + b_q) \in \mathbb{R}^d, \quad (7)$$

where  $u_X = \psi(X)$  and  $c_S = g(S)$  originate from the aforementioned multimodal encoder and text encoder, respectively;  $\oplus$  denotes the concatenation operation;  $W_q$  and  $b_q$  are trainable projection parameters; and  $\sigma(\cdot)$  is a non-linear activation function.

**Metric Learning and Sparse Aggregation.** For each entry  $d_i$  in the knowledge base, we extract its key vector  $k_i$  and value vector  $v_i$ . We compute the cosine similarity score  $s_i = \langle q, k_i \rangle / \kappa$  between the query  $q$  and key  $k_i$ , where  $\kappa$  is a temperature coefficient. Subsequently, we select the set of Top- $K$  most relevant indices  $\mathcal{N}_K$  and compute sparse attention weights:

$$\alpha_i = \frac{\exp(s_i)}{\sum_{j \in \mathcal{N}_K} \exp(s_j)}, \quad E = \sum_{i \in \mathcal{N}_K} \alpha_i v_i. \quad (8)$$

The resulting  $E$  serves as the weighted aggregated non-parametric evidence representation, effectively expanding the generative model's working memory.

**Evidence-Plan Alignment Constraint.** Retrieving based solely on vector similarity may yield evidence that is “superficially similar but semantically mismatched.” To prevent this, we impose a lightweight alignment cost, enforcing the retrieved entries to be semantically faithful to the plan. Let  $u_i = g(d_i)$  be the semantic embedding of the entry:

$$\mathcal{C}_{\text{evi}}(S, E) = \sum_{i \in \mathcal{N}_K} \alpha_i (1 - \cos(c_S, u_i)). \quad (9)$$

By minimizing this cost, we ensure that the retrieved feature anchors match not only in visual/acoustic patterns but also align precisely with the logical intent of the plan. The final retrieval output is formalized as  $(E, \mathcal{N}_K) = \pi_{\mathcal{R}}(X, S; \mathcal{D})$ .

### 3.5 Instruction-Following Executor ( $\mathcal{E}$ ): Dual-Constrained Denoising

The Executor ( $\mathcal{E}$ ) performs the **Execution** phase of trajectory  $\tau$ , translating the observation features  $u_X$ , semantic plan  $c_S$ , and concrete evidence  $E$  into the final reconstruction  $\hat{Y}$ . We model this generation as a Conditional Latent Diffusion Process.

**Latent Space States and Actions.** To reduce computational complexity, we compress the target data into a latent variable  $z_0 = \mathcal{E}_{\text{vae}}(Y)$  using a pre-trained VAE encoder. The forward process generates noisy states  $z_t = \sqrt{\bar{\alpha}_t} z_0 + \sqrt{1 - \bar{\alpha}_t} \epsilon$ , where  $\bar{\alpha}_t$  denotes the noise schedule parameter. The executor learns an action function (noise predictor):

$$\hat{\epsilon}_t = \epsilon_{\theta}(z_t, t; u_X, c_S, E), \quad \text{where } u_X = \psi(X), c_S = g(S), \quad (10)$$

This yields the single-step state transition (conditional denoising action):

$$z_{t-1} = \frac{1}{\sqrt{\bar{\alpha}_t}} \left( z_t - \frac{1 - \alpha_t}{\sqrt{1 - \bar{\alpha}_t}} \hat{\epsilon}_t \right) + \sigma_t \xi, \quad \xi \sim \mathcal{N}(0, \mathbf{I}). \quad (11)$$

Here,  $\alpha_t$  and  $\sigma_t$  represent the variance schedule parameter and posterior standard deviation at timestep  $t$ , respectively. Inference iterates from  $z_T \sim \mathcal{N}(0, \mathbf{I})$  to  $z_0^*$  and decodes the output via  $\hat{Y} = \mathcal{D}_{\text{vae}}(z_0^*)$ .

**Dual-Conditioning Injection.** To orthogonalize semantics and details within the feature space, we employ a hierarchical injection mechanism based on feature abstraction levels. Let  $h_{\ell}$  be the feature map at layer  $\ell$ :

(1) **Global Consistency (Deep Layers):** The plan condition  $c_S$  (defined in Sec 3.3) is injected via Cross-Attention into deep layers  $\mathcal{L}_{\text{deep}}$  to guide the global structure and tone:

$$h_{\ell}^+ = h_{\ell} + \text{CA}_{\ell}(h_{\ell}, c_S), \quad \ell \in \mathcal{L}_{\text{deep}}. \quad (12)$$

(2) **Local Statistics (Shallow Layers):** The evidence  $E$  (defined in Sec 3.4) is injected via Zero-Adapters into shallow layers  $\mathcal{L}_{\text{shallow}}$  to supplement texture and details:

$$h_{\ell}^+ = h_{\ell} + \text{ZA}_{\ell}(h_{\ell}, E), \quad \ell \in \mathcal{L}_{\text{shallow}}. \quad (13)$$

Here, the trainable parameters  $\phi_{\text{za}}$  of the Zero-Adapter are initialized to zero to preserve pre-trained priors during early training. This hierarchical design effectively prevents mutual interference between abstract intent (Plan) and concrete details (Evidence).

**Instruction-Following Regularization.** To ensure strict adherence to complex conditional instructions, we introduce two consistency losses. Let  $\varphi(\cdot)$  be a low-level feature extractor (e.g., shallow VGG) and  $A(\cdot)$  be an evidence alignment head (a learnable projection):

$$\mathcal{L}_{\text{plan}} = 1 - \cos(g(\hat{Y}), c_S), \quad \mathcal{L}_{\text{evi}} = \|\varphi(\hat{Y}) - A(E)\|_1. \quad (14)$$

These terms constrain the output to maintain semantic consistency and statistically match the evidence, respectively, reinforcing adherence to dual constraints.

### 3.6 Joint Optimization Objective

To balance imputation fidelity with downstream discriminative power, we employ a multi-task framework enabling end-to-end training via one-step estimation.

**1. Reconstruction Loss.** We optimize the conditional denoising distribution by minimizing a composite error. Combining the standard noise prediction term with regularization from Sec. 3.5, the total reconstruction loss is:

$$\mathcal{L}_{\text{rec}} = \mathbb{E}_{z,t,\epsilon} \left[ \|\epsilon - \epsilon_\theta(z_t, t; u_X, c_S, E)\|_2^2 \right] + \lambda_p \mathcal{L}_{\text{plan}} + \lambda_e \mathcal{L}_{\text{evi}}. \quad (15)$$

Here,  $\lambda_{p,e}$  weight the semantic and evidence constraints, ensuring physical and logical consistency of the generation.

**2. Downstream Task Loss.** To enforce “Task-Awareness,” we compute the differentiable one-step estimate  $\hat{z}_{0|t}$  of the original latent  $z_0$  via Tweedie’s formula, bypassing the non-differentiable sampling loop:

$$\hat{z}_{0|t} = \frac{1}{\sqrt{\bar{\alpha}_t}} (z_t - \sqrt{1 - \bar{\alpha}_t} \epsilon_\theta(z_t, t; u_X, c_S, E)), \quad (16)$$

where  $\bar{\alpha}_t$  is the noise schedule parameter. This estimate is fused with observation  $u_X$  and fed into classifier  $f_\phi$  to compute Cross-Entropy loss:

$$\mathcal{L}_{\text{task}} = \mathbb{E}_{z,t,y} \left[ \mathcal{L}_{\text{ce}} \left( f_\phi \left( \text{Fusion}(u_X, \hat{z}_{0|t}) \right), y \right) \right]. \quad (17)$$

where  $y$  denotes the ground-truth label and Fusion represents concatenation or pooling. This forces the generated features to be semantically complementary to the observation.

**3. Total Objective.** The unified objective balances generation and discrimination:

$$\mathcal{L}_{\text{total}} = \mathcal{L}_{\text{rec}} + \lambda_{\text{task}} \mathcal{L}_{\text{task}}. \quad (18)$$

where  $\lambda_{\text{task}}$  controls the trade-off. Minimizing  $\mathcal{L}_{\text{total}}$  achieves a closed loop where “generation serves understanding.”

## 4 Experiment

### 4.1 Experiment Settings

**Datasets and Evaluation Metrics.** Our experiments are conducted on two widely used multimodal sentiment analysis benchmarks, namely CMU-MOSI [Zadeh *et al.*, 2016] (2,199 video clips, split into 1,284/229/686 for training, validation, and testing) and CMU-MOSEI [Zadeh *et al.*, 2018] (22,856 clips with 16,326/1,871/4,659 samples for train/val/test, respectively). Both datasets annotate sentiment using continuous scores ranging from  $-3$  to  $3$ . In line with existing studies, we adopt 7-class accuracy ( $ACC_7$ ), binary accuracy ( $ACC_2$ ), and F1 score as the primary evaluation metrics.

**Baselines.** We compare our method with state-of-the-art baselines from two categories. The first group consists of recovery-based approaches, including SMCMSA [Sun *et al.*, 2024], IMDer [Wang *et al.*, 2023b], DiCMoR [Wang *et al.*, 2023a], MMIN [Zhao *et al.*, 2021], MCTN [Pham *et al.*, 2019], CRA [Tran *et al.*, 2017], and AE [Hinton and Salakhutdinov, 2006]. The second group includes non-recovery methods, namely PMSM [Liu *et al.*, 2025], CorrKD [Li *et al.*, 2024], MPLMM [Lee *et al.*, 2023], MPMM [Guo *et al.*, 2024], TATE [Zeng *et*

*al.*, 2022], DCCAE [Wang *et al.*, 2015], DCCA [Andrew *et al.*, 2013], and CCA [Hotelling, 1992].

**Experimental Protocol.** We study missing-modality scenarios across language ( $l$ ), vision ( $v$ ), and acoustics ( $a$ ) under two settings. (i) *Fixed Missingness*, where predefined modality pairs  $(l, v)$ ,  $(l, a)$ , and  $(v, a)$  are systematically removed; and (ii) *Random Missingness*, where the subset of available modalities is randomly sampled for each instance. The degree of missingness is measured by the *Missing Rate*:  $MR = 1 - \frac{1}{NM} \sum_{i=1}^N m_i$ , where  $m_i$  denotes the number of observed modalities for the  $i$ -th sample,  $N$  is the total number of samples, and  $M$  is the total number of modalities. Experiments are conducted on CMU-MOSI and CMU-MOSEI with  $MR \in \{0.0, 0.1, \dots, 0.7\}$ ; given three modalities, the maximum attainable missing rate is  $2/3 \approx 0.67$ .

**Implementation Details.** We adopt pre-extracted multimodal representations as model inputs. Specifically, BERT [Devlin *et al.*, 2019] for language ( $\mathbb{R}^{768}$ ), Facet [De la Torre and Cohn, 2011] for vision (35 facial action units), and COVAREP [Deogtess *et al.*, 2014] for acoustics ( $\mathbb{R}^{74}$ ). All models are optimized with Adam, using an initial learning rate of  $2e-3$ , which is reduced by a factor of two when the validation loss fails to improve for 10 consecutive epochs. The batch size is set to 32 for CMU-MOSI and 128 for CMU-MOSEI. For the Semantic Planner, we employ Qwen2.5-Omni [Xu *et al.*, 2025] as the backbone to process the raw data features. In the planning stage, the penalty coefficient and semantic consistency term are set to  $\lambda_s = 0.3$  and  $\gamma = 0.1$ . The semantic consistency loss and evidence alignment loss are weighted by  $\lambda_p = 0.1$  and  $\lambda_e = 0.1$ . All experiments are conducted on a machine equipped with a 12-core Intel Xeon® Gold 6342 CPU, a single NVIDIA RTX 4090 GPU, and 1 TB RAM. Results are averaged over five runs with different random seeds. For more implementation details, please refer to Appendix A.

### 4.2 Comparison with the State-of-the-art

As shown in Table 1, OMG-Agent achieves the best or tied-best results on  $ACC_2$  and  $F_1$  across all fixed-missing settings on CMU-MOSI and CMU-MOSEI, while also improving  $ACC_7$ . The advantages are particularly evident under the most challenging conditions. When only a single modality is available ( $\text{XXO}$ ), OMG-Agent outperforms the strongest baseline in  $ACC_2$  by 1.7% on CMU-MOSI and CMU-MOSEI. When the dominant language modality is absent ( $\text{XOO}$ ), the performance gaps further increase to around 1.8% and 4.1%, respectively. Notably, even in the fully observed setting ( $\text{OOO}$ ), OMG-Agent continues to outperform competing methods, achieving about 3.2% and 1.6% higher  $ACC_2$  on MOSI and MOSEI, respectively, and also obtaining superior  $ACC_7$  (48.3% and 56.5%). These results demonstrate that improved robustness under missing modalities does not compromise performance in the complete-modality scenario.

Comparable patterns are observed under random missingness (Fig. 3). Our OMG-Agent consistently outperforms competing methods across different missing rates, with the margin over CorrKD becoming more pronounced at higher levels of missingness (e.g., +3.9% on  $ACC_7$  and +4.5% on  $ACC_2$  on CMU-MOSI in the  $MR=0.7$  setting). These observations confirm the effectiveness of the proposed OMG-Agent design. By

Table 1: Results of the fixed-missing protocol on CMU-MOSI and CMU-MOSEI. “L”, “V”, and “A” denote language, vision, and audio modalities;  $\bigcirc$  and  $\times$  indicates available and missing modalities. **Bold** and underline mark the best and second-best scores.

Dataset		CMU-MOSI																				
Modalities		L V A ( $\times \times \bigcirc$ )				L V A ( $\times \bigcirc \times$ )				L V A ( $\bigcirc \times \times$ )				L V A ( $\times \bigcirc \bigcirc$ )								
Method		$ACC_2 / F1 / ACC_7$		$ACC_2 / F1 / ACC_7$		$ACC_2 / F1 / ACC_7$		$ACC_2 / F1 / ACC_7$		$ACC_2 / F1 / ACC_7$		$ACC_2 / F1 / ACC_7$		$ACC_2 / F1 / ACC_7$		$ACC_2 / F1 / ACC_7$						
Recovery	AE	49.9	47.6	15.9	52.9	50.1	16.2	79.0	79.1	28.5	55.7	54.1	17.1	80.8	80.5	39.6	82.0	79.4	42.1	82.6	82.6	44.0
	CRA	54.5	50.8	16.2	56.1	53.1	16.5	83.2	82.7	39.9	59.8	57.7	17.8	83.3	83.0	40.8	82.9	83.3	43.8	83.9	83.8	44.4
	MCTN	56.1	54.5	16.5	55.0	54.4	16.3	79.1	79.2	41.0	57.5	57.4	16.8	81.0	81.0	43.2	81.1	81.2	42.1	81.4	81.5	43.4
	MMIN	55.3	51.5	15.5	57.0	54.0	15.5	83.8	83.8	41.6	60.4	58.5	19.5	84.0	84.0	42.3	83.8	83.9	42.0	84.6	84.4	44.8
	DiCMoR	60.5	60.8	20.9	62.2	60.2	20.9	84.5	84.4	44.3	64.0	63.5	21.9	85.5	85.5	44.6	83.5	85.4	45.2	85.7	85.6	45.3
	IMDer	62.0	62.2	<u>22.0</u>	61.3	60.8	<u>22.2</u>	84.8	84.7	<u>44.8</u>	63.6	63.4	23.8	85.4	85.3	<u>45.0</u>	85.5	85.4	<u>45.3</u>	85.7	85.6	45.3
	SMCMSA	60.2	60.4	18.6	60.2	60.4	18.6	81.4	81.2	31.3	63.3	63.5	17.8	81.4	80.7	<u>37.2</u>	83.1	82.9	<u>33.2</u>	85.8	<u>86.1</u>	39.2
Non-Recovery	CCA	48.4	44.4	16.0	48.8	45.6	16.2	76.3	75.7	29.6	52.1	51.0	16.8	76.2	75.6	30.0	75.5	75.9	31.1	77.0	76.6	30.4
	DCCA	50.5	46.1	16.3	47.7	41.5	16.6	73.6	73.8	30.2	50.8	46.4	16.6	74.7	74.8	29.7	74.9	75.0	30.3	75.3	75.4	30.5
	DCCAE	48.8	42.1	16.9	52.6	51.1	17.1	76.4	76.5	28.3	54.0	52.5	17.4	77.0	77.0	30.2	76.7	76.8	30.0	77.3	77.4	31.2
	TATE	59.4	55.8	17.8	60.9	58.0	18.1	85.7	85.6	42.9	64.2	62.9	18.2	85.8	85.4	43.8	86.1	85.7	43.6	85.1	85.2	45.1
	MPMM	57.3	59.4	17.1	58.6	59.1	17.3	79.8	80.1	38.8	60.5	61.3	18.1	79.9	79.8	32.5	80.7	80.9	40.8	82.4	82.1	43.7
	MPLMM	<u>62.7</u>	<u>63.7</u>	17.3	<u>63.1</u>	<u>63.7</u>	17.8	80.1	80.3	39.5	<u>65.0</u>	<u>65.4</u>	19.9	80.8	81.1	38.7	81.1	81.2	41.5	81.6	81.5	43.5
	PMSM	59.7	53.7	18.8	62.0	61.1	20.1	<u>86.7</u>	<u>86.5</u>	39.1	61.1	59.1	22.7	85.7	<u>85.5</u>	41.7	85.7	85.6	41.4	86.0	86.0	44.5
Ours	CorrKD	60.1	47.7	21.9	59.6	52.9	19.0	85.2	85.1	44.2	64.0	64.1	18.5	85.1	85.0	44.2	85.3	85.2	44.1	<u>86.0</u>	86.0	45.1
	Ours	<b>64.4</b>	<b>63.9</b>	<b>22.6</b>	<b>65.7</b>	<b>65.5</b>	<b>23.1</b>	<b>86.7</b>	<b>86.6</b>	<b>45.3</b>	<b>66.8</b>	<b>64.7</b>	<b>25.6</b>	<b>86.6</b>	<b>86.6</b>	<b>47.2</b>	<b>87.3</b>	<b>87.1</b>	<b>48.0</b>	<b>89.2</b>	<b>89.1</b>	<b>48.3</b>

Dataset		CMU-MOSEI																				
Modalities		L V A ( $\times \times \bigcirc$ )				L V A ( $\times \bigcirc \times$ )				L V A ( $\bigcirc \times \times$ )				L V A ( $\times \bigcirc \bigcirc$ )								
Method		$ACC_2 / F1 / ACC_7$		$ACC_2 / F1 / ACC_7$		$ACC_2 / F1 / ACC_7$		$ACC_2 / F1 / ACC_7$		$ACC_2 / F1 / ACC_7$		$ACC_2 / F1 / ACC_7$		$ACC_2 / F1 / ACC_7$		$ACC_2 / F1 / ACC_7$						
Recovery	AE	52.2	52.5	40.1	49.0	44.9	37.9	75.3	75.4	45.4	56.9	55.3	39.7	76.2	76.3	46.0	76.7	76.3	45.8	77.2	77.3	46.8
	CRA	51.5	52.3	39.8	48.4	44.3	37.5	75.2	75.0	45.8	55.7	54.2	39.8	76.0	75.5	46.2	76.5	76.2	45.7	76.4	76.8	47.1
	MCTN	62.7	54.5	41.4	62.6	57.1	41.6	82.6	82.8	50.2	63.7	62.7	42.1	83.5	83.3	50.7	83.2	83.2	50.4	84.2	84.2	51.2
	MMIN	58.9	59.5	40.4	59.3	60.0	40.7	82.3	82.4	51.4	63.5	61.9	41.8	83.7	83.3	52.0	83.8	83.4	51.2	84.3	84.2	52.4
	DiCMoR	62.9	60.4	41.4	63.6	63.6	42.0	84.2	84.3	52.4	65.2	64.4	42.4	85.0	84.9	52.7	84.9	84.9	53.0	85.1	85.1	53.4
	IMDer	63.8	60.6	<u>41.7</u>	63.8	60.6	41.7	84.5	84.5	<u>52.5</u>	63.5	64.9	42.8	85.1	<u>53.1</u>	85.0	85.0	<u>53.1</u>	85.1	85.1	<u>53.4</u>	
	SMCMSA	63.3	67.5	41.4	64.2	63.3	<b>48.7</b>	80.3	80.6	50.8	65.5	64.8	<b>49.3</b>	76.5	76.3	44.6	75.9	76.3	48.2	80.6	80.9	50.7
Non-Recovery	CCA	54.8	55.0	39.5	50.7	47.2	38.3	78.2	77.5	46.8	58.9	57.8	40.1	79.7	78.6	46.3	78.9	79.3	46.0	79.8	79.6	47.3
	DCCA	62.0	50.2	41.1	61.9	55.7	41.3	79.7	79.5	47.0	63.4	65.9	41.5	79.5	79.2	46.7	80.3	79.7	46.6	80.7	80.9	47.7
	DCCAE	61.4	53.8	40.9	61.1	57.2	40.1	78.5	78.7	46.7	62.7	59.2	41.6	80.0	80.0	47.4	80.4	80.4	47.1	81.2	81.2	48.2
	TATE	65.5	65.2	41.0	62.5	61.2	41.8	82.8	82.5	51.8	64.1	62.8	41.8	84.1	84.2	51.5	83.9	83.8	51.5	84.9	84.4	52.5
	MPMM	66.9	68.7	41.2	67.2	69.3	43.5	78.2	78.3	46.9	68.1	69.8	43.5	79.4	79.5	46.4	79.6	79.7	46.2	80.6	80.8	47.8
	MPLMM	<u>67.3</u>	<u>68.7</u>	41.3	<u>67.3</u>	<u>69.4</u>	43.7	79.1	79.2	47.2	<u>68.2</u>	<u>69.9</u>	43.9	80.5	80.4	47.5	80.1	80.1	47.3	81.1	81.4	48.4
	PMSM	62.9	48.5	41.4	62.9	48.5	41.4	84.8	84.7	52.2	64.8	51.0	44.6	85.3	85.1	50.1	85.1	85.0	51.4	85.1	84.8	51.7
Ours	CorrKD	64.9	62.3	41.2	65.5	64.0	41.4	<u>85.6</u>	<u>85.3</u>	51.4	65.5	64.0	41.4	<u>85.7</u>	<u>85.6</u>	52.5	85.7	<u>85.6</u>	52.1	<u>85.7</u>	<u>85.6</u>	52.0
	Ours	<b>69.0</b>	<b>69.7</b>	<b>44.2</b>	<b>68.0</b>	<b>69.8</b>	<b>45.8</b>	<b>87.3</b>	<b>87.1</b>	<b>53.5</b>	<b>72.3</b>	<b>72.2</b>	<b>47.2</b>	<b>86.4</b>	<b>86.7</b>	<b>53.3</b>	<b>86.3</b>	<b>86.5</b>	<b>54.4</b>	<b>87.3</b>	<b>87.4</b>	<b>56.5</b>

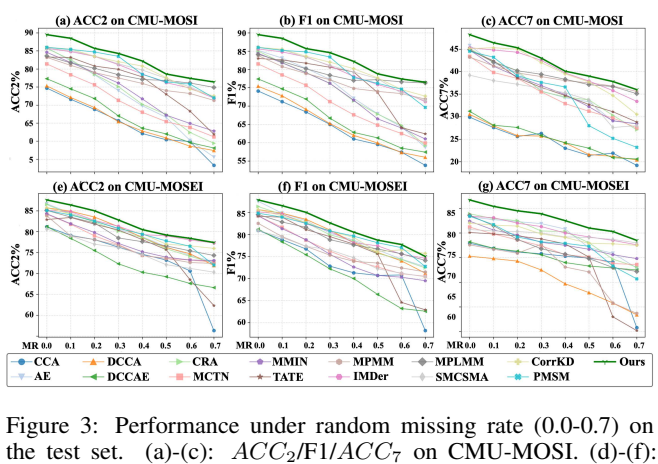


Figure 3: Performance under random missing rate (0.0-0.7) on the test set. (a)-(c):  $ACC_2 / F1 / ACC_7$  on CMU-MOSI. (d)-(f):  $ACC_2 / F1 / ACC_7$  on CMU-MOSEI.

explicitly reformulating missing-modality reconstruction as a Planning-Retrieval-Execution cognitive trajectory, the model mitigates the semantic-signal entanglement in static end-to-end mappings. The structured semantic plan provides global guidance, retrieved non-parametric evidence anchors the generation to concrete features and suppresses off-manifold artifacts, and dual consistency constraints during execution further reduce the influence of unreliable surrogate modalities, leading to more stable and well-calibrated predictions under high

missing rates.

Table 2: Performance comparison ( $ACC_2 / F1 / ACC_7$ ) under the fixed-missing protocol. The best results are highlighted in **bold**.

Dataset		$ACC_2 / F1 / ACC_7$															
Modalities		L V A ( $\times \times \bigcirc$ )				L V A ( $\times \bigcirc \times$ )				L V A ( $\bigcirc \times \times$ )				L V A ( $\times \bigcirc \bigcirc$ )			
Method																	

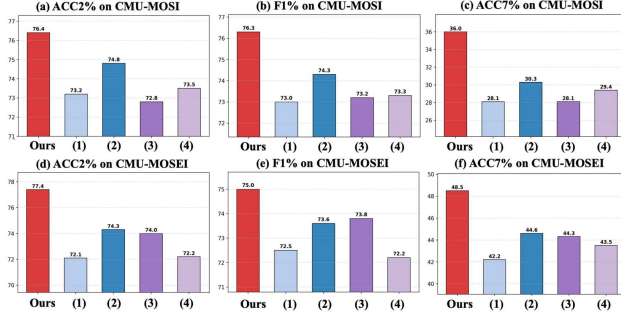


Figure 4: Ablation study of OMG-Agent architecture on the test set (MR=0.7). We report  $ACC_2$ / $F1$ / $ACC_7$  scores on CMU-MOSI (a-c) and CMU-MOSEI (d-f).

logical decomposition for resolving cross-modal ambiguity; (ii) w/o Re-ranking, which retains planning generation but removes candidate re-ranking, leading to a  $ACC_2$  drop of 1.6% and 3.1%, indicating that optimized planning aids precise sentiment localization; (iii) w/o Retriever, which cuts off external knowledge base access, leading to a  $ACC_2$  drop of 3.6% and 3.4%; and (iv) w/o Sparse Attn, replacing sparse aggregation with mean pooling, resulting in a  $ACC_2$  drop of 2.9% and 5.2%. This confirms that non-parametric evidence requires relevance-based weighting to effectively introduce fine-grained sentiment features.

Table 3: Ablation study on Instruction-Following Regularization and Task-Aware Optimization (MR=0.7). The results are reported in  $ACC_2$  /  $F1$  /  $ACC_7$ .

Variants	CMU-MOSI	CMU-MOSEI
<b>Ours</b>	<b>76.4 / 76.3 / 36.0</b>	<b>77.4 / 75.0 / 48.5</b>
<i>Instruction-Following Regularization</i>		
w/o $\mathcal{L}_{\text{plan}}$	72.8 / 73.1 / 33.2	74.5 / 74.5 / 46.2
w/o $\mathcal{L}_{\text{evi}}$	71.9 / 72.0 / 32.7	73.2 / 72.7 / 44.1
w/o Both	70.3 / 70.1 / 28.4	72.4 / 73.0 / 43.3
<i>Task-Aware Optimization</i>		
w/o $\mathcal{L}_{\text{task}}$	71.8 / 71.2 / 33.4	72.0 / 72.7 / 38.5
Direct Classification	72.2 / 71.3 / 30.3	75.4 / 74.3 / 46.7

**Necessity of Instruction-Following Regularization** To investigate the impact of regularization terms on sentiment consistency, we decomposed the loss function: (i) w/o  $\mathcal{L}_{\text{plan}}$ , which produced features with reasonable context but deviated sentiment intensity; (ii) w/o  $\mathcal{L}_{\text{evi}}$ , which lacked fine-grained sentiment cues, affecting hard sample classification; and (iii) w/o Both, leading to severe “Conditioning Neglect” and a sharp  $ACC_2$  drop of 6.1% and 5.0% as shown in Table 3. This demonstrates that  $\mathcal{L}_{\text{plan}}$  ensures polarity correctness, while  $\mathcal{L}_{\text{evi}}$  enhances expressive nuance.

**Manifold Projection via Task-Aware Optimization** To validate the role of the joint optimization objective, we compared three strategies, as shown in Table 3: (i) w/o  $\mathcal{L}_{\text{task}}$ , training with reconstruction loss only, yielding a  $ACC_2$  of 71.8% and 72.0%, (ii) Direct Classification, applying task-loss directly to the noisy state and (iii) Tweedie. A key

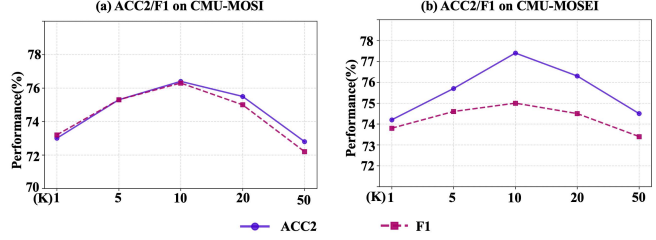


Figure 5: Ablation study of retrieval quantity  $K$ . We report  $ACC$ / $F1$  on CMU-MOSI (a) and CMU-MOSEI (b).

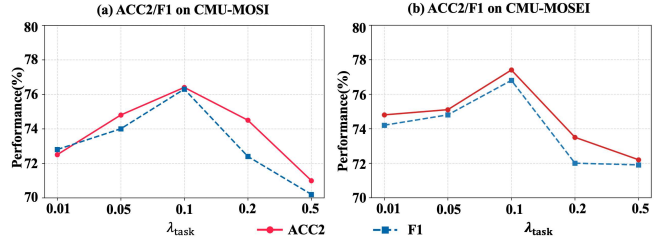


Figure 6: Ablation study of task weight  $\lambda_{\text{task}}$ . We report  $ACC$ / $F1$  on CMU-MOSI (a) and CMU-MOSEI (b).

finding is that Direct Classification improves performance negligibly ( $ACC_2$ : 0.4) on CMU-MOSI as noise blurs decision boundaries. Tweedie’s formula successfully projects states back to the clean data manifold, enabling the classifier to provide accurate semantic gradients, boosting  $ACC_2$  to 76.4% and 77.4%, which proves the mechanism’s importance for generating discriminative features.

**Hyperparameter Sensitivity and Trade-offs** We investigate the impact of critical hyperparameters and the result is shown in Figure 5 and Figure 6. For retrieval quantity  $K$ ,  $ACC_2$  and F1 follows an inverted U-shaped trend, peaking at  $K = 10$ ; excessive  $K$  introduces sentiment-irrelevant redundancy that interferes with classification. For task weight  $\lambda_{\text{task}}$ , a moderate weight ( $\lambda_{\text{task}} = 0.1$ ) significantly improves all metrics by adapting generated features to the downstream task. However, excessive weight leads to overfitting the training distribution, where generated features lose natural modal characteristics, degrading test set performance. For more ablation results, please refer to Appendix D.

## 5 Conclusion

In this paper, we propose **OMG-Agent**, a novel framework that redefines missing modality reconstruction as a dynamic coarse-to-fine Agentic Workflow. By explicitly decoupling the generation process into Progressive Contextual Reasoning, active evidence grounding, and instruction-following execution, we effectively resolve the Semantic-Detail Entanglement challenge inherent in traditional end-to-end models. Extensive experiments on multiple datasets confirm its state-of-the-art performance, particularly under high missing rates. Future work will focus on optimizing inference efficiency through agentic knowledge distillation, integrating dynamic web-scale retrieval mechanisms to overcome static database limitations, and extending the framework to a broader spectrum of modalities and downstream tasks.

## Acknowledgments

## References

[Andrew *et al.*, 2013] Galen Andrew, Raman Arora, Jeff Bilmes, and Karen Livescu. Deep canonical correlation analysis. In *International conference on machine learning*, pages 1247–1255. PMLR, 2013.

[Asai *et al.*, 2024] Akari Asai, Zeqiu Wu, Yizhong Wang, Avirup Sil, and Hannaneh Hajishirzi. Self-rag: Learning to retrieve, generate, and critique through self-reflection. 2024.

[De la Torre and Cohn, 2011] Fernando De la Torre and Jeffrey F Cohn. Facial expression analysis. *Visual analysis of humans: Looking at people*, pages 377–409, 2011.

[Degottex *et al.*, 2014] Gilles Degottex, John Kane, Thomas Drugman, Tuomo Raitio, and Stefan Scherer. Covarep—a collaborative voice analysis repository for speech technologies. In *2014 ieee international conference on acoustics, speech and signal processing (icassp)*, pages 960–964. IEEE, 2014.

[Devlin *et al.*, 2019] Jacob Devlin, Ming-Wei Chang, Kenton Lee, and Kristina Toutanova. Bert: Pre-training of deep bidirectional transformers for language understanding. In *Proceedings of the 2019 conference of the North American chapter of the association for computational linguistics: human language technologies, volume 1 (long and short papers)*, pages 4171–4186, 2019.

[Fan *et al.*, 2025] Hongxing Fan, Shuyu Zhao, Jiayang Ao, and Lu Sheng. Reasoning-driven amodal completion: Collaborative agents and perceptual evaluation. *arXiv preprint arXiv:2512.20936*, 2025.

[Gao *et al.*, 2025] Silin Gao, Jane Dwivedi-Yu, Ping Yu, Xiaojing Ellen Tan, Ramakanth Pasunuru, Olga Golovneva, Koustuv Sinha, Asli Celikyilmaz, Antoine Bosselut, and Tianlu Wang. Efficient tool use with chain-of-abstraction reasoning. In *Proceedings of the 31st International Conference on Computational Linguistics*, pages 2727–2743, 2025.

[Guo *et al.*, 2024] Zirun Guo, Tao Jin, and Zhou Zhao. Multimodal prompt learning with missing modalities for sentiment analysis and emotion recognition. *arXiv preprint arXiv:2407.05374*, 2024.

[Hinton and Salakhutdinov, 2006] Geoffrey E Hinton and Ruslan R Salakhutdinov. Reducing the dimensionality of data with neural networks. *science*, 313(5786):504–507, 2006.

[Hotelling, 1992] Harold Hotelling. Relations between two sets of variates. In *Breakthroughs in statistics: methodology and distribution*, pages 162–190. Springer, 1992.

[Huang *et al.*, 2025] Lun Huang, You Xie, Hongyi Xu, Tianpei Gu, Chenxu Zhang, Guoxian Song, Zenan Li, Xiaochen Zhao, Linjie Luo, and Guillermo Sapiro. Plan-x: Instruct video generation via semantic planning. *arXiv preprint arXiv:2511.17986*, 2025.

[Kang *et al.*, 2023] Minguk Kang, Jun-Yan Zhu, Richard Zhang, Jaesik Park, Eli Shechtman, Sylvain Paris, and Taesung Park. Scaling up gans for text-to-image synthesis. In *Proceedings of the IEEE/CVF conference on computer vision and pattern recognition*, pages 10124–10134, 2023.

[Lee *et al.*, 2023] Yi-Lun Lee, Yi-Hsuan Tsai, Wei-Chen Chiu, and Chen-Yu Lee. Multimodal prompting with missing modalities for visual recognition. In *Proceedings of the IEEE/CVF Conference on Computer Vision and Pattern Recognition*, pages 14943–14952, 2023.

[Li *et al.*, 2024] Mingcheng Li, Dingkang Yang, Xiao Zhao, Shuaibing Wang, Yan Wang, Kun Yang, Mingyang Sun, Dongliang Kou, Ziyun Qian, and Lihua Zhang. Correlation-decoupled knowledge distillation for multimodal sentiment analysis with incomplete modalities. In *Proceedings of the IEEE/CVF Conference on Computer Vision and Pattern Recognition*, pages 12458–12468, 2024.

[Liu *et al.*, 2023] Haotian Liu, Chunyuan Li, Qingyang Wu, and Yong Jae Lee. Visual instruction tuning. *Advances in neural information processing systems*, 36:34892–34916, 2023.

[Liu *et al.*, 2025] Jiaqi Liu, Yong Wang, Jing Yang, Fanshu Shang, and Fan He. Prompt-matching synthesis model for missing modalities in sentiment analysis. *Knowledge-Based Systems*, page 113519, 2025.

[Ma *et al.*, 2021] Mengmeng Ma, Jian Ren, Long Zhao, Sergey Tulyakov, Cathy Wu, and Xi Peng. Smil: Multimodal learning with severely missing modality. In *Proceedings of the AAAI conference on artificial intelligence*, volume 35, pages 2302–2310, 2021.

[Nguyen *et al.*, 2025] Pha Nguyen, Sailik Sengupta, Girik Malik, Arshit Gupta, and Bonan Min. Install: Context-aware instructional task assistance with multi-modal large language models. *arXiv preprint arXiv:2501.12231*, 2025.

[Palumbo *et al.*, 2023] Emanuele Palumbo, Imant Daunhawer, and Julia E Vogt. Mmvae+: Enhancing the generative quality of multimodal vaes without compromises. In *The Eleventh International Conference on Learning Representations*. OpenReview, 2023.

[Pham *et al.*, 2019] Hai Pham, Paul Pu Liang, Thomas Manzini, Louis-Philippe Morency, and Barnabás Póczos. Found in translation: Learning robust joint representations by cyclic translations between modalities. In *Proceedings of the AAAI conference on artificial intelligence*, volume 33, pages 6892–6899, 2019.

[Rawat *et al.*, 2025] Mrinal Rawat, Ambuje Gupta, Rushil Goomer, Alessandro Di Bari, Neha Gupta, and Roberto Pieraccini. Pre-act: Multi-step planning and reasoning improves acting in llm agents. *arXiv preprint arXiv:2505.09970*, 2025.

[Rombach *et al.*, 2022] Robin Rombach, Andreas Blattmann, Dominik Lorenz, Patrick Esser, and Björn Ommer. High-resolution image synthesis with latent diffusion models. In *Proceedings of the IEEE/CVF conference on computer vision and pattern recognition*, pages 10684–10695, 2022.

[Schick *et al.*, 2023] Timo Schick, Jane Dwivedi-Yu, Roberto Dessì, Roberta Raileanu, Maria Lomeli, Eric Hambro, Luke Zettlemoyer, Nicola Cancedda, and Thomas Scialom. Toolformer: Language models can teach themselves to use tools. *Advances in Neural Information Processing Systems*, 36:68539–68551, 2023.

[Sharma *et al.*, 2025] Kartik Sharma, Peeyush Kumar, and Yunqing Li. Og-rag: ontology-grounded retrieval-augmented generation for large language models. In *Proceedings of the 2025 Conference on Empirical Methods in Natural Language Processing*, pages 32950–32969, 2025.

[Song *et al.*, 2025] Hwanjun Song, Jeonghwan Choi, and Minseok Kim. Ext2gen: Alignment through unified extraction and generation for robust retrieval-augmented generation. *arXiv preprint arXiv:2503.04789*, 2025.

[Sun *et al.*, 2024] Yuhang Sun, Zhizhong Liu, Quan Z Sheng, Dianhui Chu, Jian Yu, and Hongxiang Sun. Similar modality completion-based multimodal sentiment analysis under uncertain missing modalities. *Information Fusion*, 110:102454, 2024.

[Sutter *et al.*, 2024] Thomas Sutter, Yang Meng, Andrea Agostini, Daphné Chopard, Norbert Fortin, Julia Vogt, Babak Shahbaba, and Stephan Mandt. Unity by diversity: Improved representation learning for multimodal vaes. *Advances in Neural Information Processing Systems*, 37:74262–74297, 2024.

[Tran *et al.*, 2017] Luan Tran, Xiaoming Liu, Jiayu Zhou, and Rong Jin. Missing modalities imputation via cascaded residual autoencoder. In *Proceedings of the IEEE conference on computer vision and pattern recognition*, pages 1405–1414, 2017.

[Wang *et al.*, 2015] Weiran Wang, Raman Arora, Karen Livescu, and Jeff Bilmes. On deep multi-view representation learning. In *International conference on machine learning*, pages 1083–1092. PMLR, 2015.

[Wang *et al.*, 2023a] Yuanzhi Wang, Zhen Cui, and Yong Li. Distribution-consistent modal recovering for incomplete multimodal learning. In *Proceedings of the IEEE/CVF International Conference on Computer Vision*, pages 22025–22034, 2023.

[Wang *et al.*, 2023b] Yuanzhi Wang, Yong Li, and Zhen Cui. Incomplete multimodality-diffused emotion recognition. *Advances in Neural Information Processing Systems*, 36:17117–17128, 2023.

[Wu *et al.*, 2024] Renjie Wu, Hu Wang, Hsiang-Ting Chen, and Gustavo Carneiro. Deep multimodal learning with missing modality: A survey. *arXiv preprint arXiv:2409.07825*, 2024.

[Xu *et al.*, 2025] Jin Xu, Zhifang Guo, Jinzheng He, Hangrui Hu, Ting He, Shuai Bai, Keqin Chen, Jialin Wang, Yang Fan, Kai Dang, Bin Zhang, Xiong Wang, Yunfei Chu, and Junyang Lin. Qwen2.5-omni technical report, 2025.

[Yao *et al.*, 2022] Shunyu Yao, Jeffrey Zhao, Dian Yu, Nan Du, Izhak Shafran, Karthik R Narasimhan, and Yuan Cao. React: Synergizing reasoning and acting in language models. In *The eleventh international conference on learning representations*, 2022.

[Ye *et al.*, 2023] Qinghao Ye, Haiyang Xu, Guohai Xu, Jiabo Ye, Ming Yan, Yiyang Zhou, Junyang Wang, Anwen Hu, Pengcheng Shi, Yaya Shi, et al. mplug-owl: Modularization empowers large language models with multimodality. *arXiv preprint arXiv:2304.14178*, 2023.

[Zadeh *et al.*, 2016] Amir Zadeh, Rowan Zellers, Eli Pincus, and Louis-Philippe Morency. Mosi: multimodal corpus of sentiment intensity and subjectivity analysis in online opinion videos. *arXiv preprint arXiv:1606.06259*, 2016.

[Zadeh *et al.*, 2018] AmirAli Bagher Zadeh, Paul Pu Liang, Soujanya Poria, Erik Cambria, and Louis-Philippe Morency. Multimodal language analysis in the wild: Cmu-mosei dataset and interpretable dynamic fusion graph. In *Proceedings of the 56th Annual Meeting of the Association for Computational Linguistics (Volume 1: Long Papers)*, pages 2236–2246, 2018.

[Zang *et al.*, 2025] Yuhang Zang, Wei Li, Jun Han, Kaiyang Zhou, and Chen Change Loy. Contextual object detection with multimodal large language models. *International Journal of Computer Vision*, 133(2):825–843, 2025.

[Zeng *et al.*, 2022] Jiandian Zeng, Tianyi Liu, and Jiantao Zhou. Tag-assisted multimodal sentiment analysis under uncertain missing modalities. In *Proceedings of the 45th International ACM SIGIR Conference on Research and Development in Information Retrieval*, pages 1545–1554, 2022.

[Zhang *et al.*, 2024] Yue Zhang, Chengtao Peng, Qiuli Wang, Dan Song, Kaiyan Li, and S Kevin Zhou. Unified multimodal image synthesis for missing modality imputation. *IEEE Transactions on Medical Imaging*, 44(1):4–18, 2024.

[Zhang *et al.*, 2025] Yue Zhang, Yafu Li, Leyang Cui, Deng Cai, Lemao Liu, Tingchen Fu, Xinting Huang, Enbo Zhao, Yu Zhang, Yulong Chen, et al. Siren’s song in the ai ocean: A survey on hallucination in large language models. *Computational Linguistics*, pages 1–46, 2025.

[Zhao *et al.*, 2021] Jinming Zhao, Ruichen Li, and Qin Jin. Missing modality imagination network for emotion recognition with uncertain missing modalities. In *Proceedings of the 59th Annual Meeting of the Association for Computational Linguistics and the 11th International Joint Conference on Natural Language Processing (Volume 1: Long Papers)*, pages 2608–2618, 2021.

# Supplementary Material: OMG-Agent: Toward Robust Missing Modality Generation with Decoupled Coarse-to-Fine Agentic Workflows

## Abstract

This supplementary material provides technical and theoretical support for **OMG-Agent**: **Appendix A** specifies implementation details and configurations; **Appendix B** presents mathematical proofs for the Trajectory Utility and the MMSE estimator; **Appendix C** details experimental setups and baseline protocols; and **Appendix D** reports additional quantitative results.

## A Implementation Details

**Comprehensive Configuration and Grid Search.** To ensure reproducibility, we detail the technical specifications of OMG-Agent. The optimization of balancing weights  $\lambda_s$ ,  $\lambda_p$ , and  $\lambda_e$  follows a multi-stage grid search on the validation set. Detailed hyperparameter configurations are summarized in Table 1. All models are optimized using the Adam optimizer with an initial learning rate of  $2 \times 10^{-3}$  and a decay factor of 0.5 triggered after 10 epochs of validation plateau. Input dimensions follow established protocols: 768 for language (BERT), 35 for vision (Facet AUs), and 74 for acoustics (COVAREP).

Table 1: Hyperparameter settings for OMG-Agent components.

Module	Parameter	Value
Global	Optimizer / Initial LR	Adam / $2 \times 10^{-3}$
	Batch Size (MOSI / MOSEI)	32 / 128
Planner $\mathcal{P}$	Penalty $\lambda_s/\gamma$	0.3 / 0.1
	Candidate Set Size $ \Omega(X) $	5
	Schema Format	Triplet [E, A, S]
Retriever $\mathcal{R}$	Retrieval Count $K$ / Temp $\kappa$	10 / 0.07
Executor $\mathcal{E}$	Consistency $\lambda_p/\lambda_e$	0.1 / 0.1
	Task-Aware Weight $\lambda_{task}$	0.1

**Planner Prompting Strategy.** The Semantic Planner  $\mathcal{P}$  utilizes a system prompt that enforces a structured triplet schema: [Entity, Action, Sentiment]. This design allows the text encoder  $g(\cdot)$  to extract deterministic logical guidance  $c_S$  from the discrete reasoning results, effectively reducing the one-to-many ambiguity inherent in cross-modal mapping. During ablation studies, the *w/o Planner* baseline is implemented by replacing  $c_S$  with Gaussian noise.

**Hardware and Inference Latency.** Experiments were executed on a machine equipped with an Intel Xeon Gold 6342 CPU and an NVIDIA RTX 4090 GPU. To optimize throughput during training, we utilize the differentiable one-step estimate  $\hat{z}_{0|t}$  via Tweedie's formula to bypass the non-differentiable sampling loop. The average end-to-end inference latency is approximately 84ms per sample, with semantic planning and retrieval-execution accounting for 45% and 55% of the total time, respectively. All reported metrics represent the average performance over five independent runs with distinct random seeds.

## B Comprehensive Mathematical Derivations

### B.1 Bayesian Step-by-Step Decomposition of Trajectory Utility

The optimization of the OMG-Agent framework is grounded in maximizing the joint posterior distribution  $p(Y, S, E | X)$ . To derive the additive Trajectory Utility  $\mathcal{U}$ , we first apply the definition of conditional probability:

$$p(Y, S, E | X) = \frac{p(Y, S, E, X)}{p(X)} \quad (1)$$

where  $Y$  is the missing target modality,  $S$  is the semantic plan,  $E$  is the retrieved evidence, and  $X$  is the partial observation. The probability  $p(X)$  is a marginal constant that does not affect the optimization of parameters.

Subsequently, the joint probability  $p(Y, S, E, X)$  can be sequentially decomposed using the probability chain rule following the causal workflow of our agent (Planning  $\rightarrow$  Retrieval  $\rightarrow$  Execution):

$$p(Y, S, E, X) = p(Y | S, E, X) \cdot p(E | S, X) \cdot p(S | X) \cdot p(X) \quad (2)$$

By substituting this expansion into the log-likelihood objective and discarding the constant term  $\log p(X)$ , we obtain the final decomposed utility function:

$$\begin{aligned} \log p(Y, S, E | X) &= \log p(Y | S, E, X) \\ &\quad + \log p(E | S, X) \\ &\quad + \log p(S | X) \end{aligned} \quad (3)$$

This derivation theoretically justifies the additive structure of the utility function used in the main text. Each log-likelihood

term represents a specific module’s objective:  $\log p(Y | S, E, X)$  corresponds to the synthesis fidelity of the Executor,  $\log p(E | S, X)$  denotes the alignment quality of the Retriever, and  $\log p(S | X)$  ensures the logical consistency of the Planner.

## B.2 Formal Derivation of the Tweedie-based MMSE Estimate

To facilitate the backpropagation of gradients from downstream discriminative tasks during the iterative denoising process, we derive the Minimum Mean Squared Error (MMSE) estimator  $\hat{z}_{0|t}$  for the clean latent  $z_0$  at any timestep  $t$ .

The forward diffusion process defines the relationship between the noisy state  $z_t$  and the original clean latent  $z_0$  as:

$$z_t = \sqrt{\bar{\alpha}_t} z_0 + \sqrt{1 - \bar{\alpha}_t} \epsilon, \quad \epsilon \sim \mathcal{N}(0, \mathbf{I}) \quad (4)$$

where  $z_t$  is the noisy latent at timestep  $t$ ,  $z_0$  is the clean latent encoded by the VAE,  $1 - \bar{\alpha}_t$  is the noise variance schedule, and  $\epsilon$  represents the injected Gaussian noise.

The derivation starts from the fundamental property relating the score function  $\nabla_{z_t} \log p(z_t)$  to the conditional expectation:

$$\nabla_{z_t} \log p(z_t) = \int p(z_0 | z_t) \nabla_{z_t} \log p(z_t | z_0) dz_0 \quad (5)$$

Since  $\frac{p(z_t | z_0)}{p(z_0 | z_t)}$  follows a Gaussian distribution  $\mathcal{N}(z_t; \sqrt{\bar{\alpha}_t} z_0, (1 - \bar{\alpha}_t) \mathbf{I})$ , its log-gradient is expressed as:

$$\nabla_{z_t} \log p(z_t | z_0) = -\frac{z_t - \sqrt{\bar{\alpha}_t} z_0}{1 - \bar{\alpha}_t} \quad (6)$$

Substituting this into the integral yields:

$$\begin{aligned} \nabla_{z_t} \log p(z_t) &= -\frac{1}{1 - \bar{\alpha}_t} \left[ z_t - \sqrt{\bar{\alpha}_t} \int z_0 p(z_0 | z_t) dz_0 \right] \\ &= -\frac{z_t - \sqrt{\bar{\alpha}_t} \mathbb{E}[z_0 | z_t]}{1 - \bar{\alpha}_t} \end{aligned} \quad (7)$$

Rearranging the terms leads to the core form of Tweedie’s Identity:

$$\mathbb{E}[z_0 | z_t] = \frac{1}{\sqrt{\bar{\alpha}_t}} (z_t + (1 - \bar{\alpha}_t) \nabla_{z_t} \log p(z_t)) \quad (8)$$

The score function is approximated by the trained conditional noise predictor  $\epsilon_\theta$  such that:

$$\nabla_{z_t} \log p(z_t) \approx -\frac{\epsilon_\theta(z_t, t; u_X, c_S, E)}{\sqrt{1 - \bar{\alpha}_t}} \quad (9)$$

Substituting this approximation into the identity gives the final differentiable estimator  $\hat{z}_{0|t}$ :

$$\hat{z}_{0|t} = \frac{1}{\sqrt{\bar{\alpha}_t}} (z_t - \sqrt{1 - \bar{\alpha}_t} \epsilon_\theta(z_t, t; u_X, c_S, E)) \quad (10)$$

where  $\hat{z}_{0|t}$  is the closed-form MMSE estimate of  $z_0$ ,  $u_X$  denotes the observed features,  $c_S$  is the semantic plan vector, and  $E$  is the retrieved evidence. This formulation establishes a differentiable path for the task loss  $\mathcal{L}_{task}$  to propagate gradients through the sampling loop to  $\epsilon_\theta$ , ensuring the Executor synthesizes features that maximize discriminative performance for downstream tasks.

## C Extended Experiment Details

### C.1 Datasets Details

We validate our method on a set of visual and multimodal benchmarks. These datasets include simple image classification tasks and complex multimodal comprehension tasks. The specific details are as follows:

- **CMU-MOSI**[Zadeh *et al.*, 2016]: A multimodal dataset designed for sentiment analysis at the opinion segment level. It consists of 2,199 annotated video clips collected from online opinion videos, each labeled with continuous sentiment intensity scores ranging from negative to positive. Similar to CMU-MOSEI, the dataset aligns three modalities: textual transcripts of speech, visual cues (facial expressions and head movements), and acoustic features (intonation and prosody). CMU-MOSI serves as a standard benchmark for evaluating multimodal fusion models in fine-grained sentiment understanding.
- **CMU-MOSEI**[Zadeh *et al.*, 2018]: A multimodal dataset used in sentiment analysis and emotion recognition tasks. It includes over 23,000 video clips, which are annotated with sentiment analysis (positive, neutral, or negative) and emotion intensity scores. The dataset aligns three modalities: textual transcripts of speech, visual signals (facial expressions and gestures), and acoustic features (vocal tone and prosody). It is a comprehensive benchmark for evaluating models’ ability to fuse linguistic, visual, and audio information to interpret human sentiment and emotion.
- **CH-SIMS**[Yu *et al.*, 2020]: A Chinese unimodal and multimodal sentiment analysis dataset consisting of 2,281 in-the-wild refined video clips with both multimodal and independent unimodal annotations. The dataset enables the study of cross-modal interactions as well as standalone unimodal sentiment analysis using modality-specific labels. It covers three aligned modalities: Chinese textual transcripts, visual signals (facial expressions and gestures), and acoustic features (prosody and vocal characteristics). CH-SIMS serves as an important benchmark for evaluating sentiment modeling in Chinese multimodal and unimodal settings.

### C.2 Datasets

- **AE**[Hinton and Salakhutdinov, 2006]: A conventional autoencoder-based reconstruction method that infers latent representations for missing modalities and decodes them to recover complete multimodal inputs. This approach is commonly adopted as a canonical recovery-first baseline.
- **CRA**[Tran *et al.*, 2017]: A cascaded residual autoencoder framework composed of multiple reconstruction stages. By progressively refining intermediate representations at each stage, it strengthens cross-modal dependency modeling and improves the accuracy of missing-modality recovery.
- **MCTN**[Pham *et al.*, 2019]: A modality translation framework that learns mappings between source and target modalities using sequence-to-sequence architectures.

Through cross-modal translation, it derives shared representations capable of substituting absent modalities.

- **MMIN**[Zhao *et al.*, 2021]: An extension of CRA that incorporates a cycle-consistency loss to preserve alignment between generated and observed modalities. These latent-level constraints enhance robustness across diverse missing-modality conditions.
- **DiCMoR**[Wang *et al.*, 2023a]: A flow-based modality completion method that leverages class-conditional normalizing flows to align distributions of incomplete modalities with those of fully observed ones. The invertible design enables accurate density matching and high-fidelity restoration.
- **IMDer**[Wang *et al.*, 2023b]: A diffusion-based imputation approach that incrementally transforms Gaussian noise into realistic missing-modality samples. By conditioning on observed modality embeddings, the diffusion process is guided toward semantically consistent completions.
- **SMCNSA**[Sun *et al.*, 2024]: A similarity-driven completion strategy that builds a repository of fully observed multimodal samples and retrieves nearest neighbors based on cosine similarity and sentiment labels. The retrieved samples are used to fill missing modalities, while decision-level fusion with pretrained encoders improves robustness under uncertain missingness.
- **CCA**[Hotelling, 1992]: A classical canonical correlation analysis technique that projects different modalities into a shared latent space by maximizing their pairwise linear correlations.
- **DCCA**[Andrew *et al.*, 2013]: An extension of CCA that replaces linear projections with deep neural networks, enabling the modeling of nonlinear cross-modal relationships and yielding more expressive representations.
- **DCCAE**[Wang *et al.*, 2015]: A hybrid framework that jointly optimizes deep CCA objectives alongside autoencoder reconstruction losses. This joint formulation encourages representations that are both structurally faithful to inputs and highly correlated across modalities.
- **TATE**[Zeng *et al.*, 2022]: A label-guided Transformer model designed to accommodate single or multiple missing modalities. It introduces shared semantic tokens and employs an encoder-decoder architecture to project multimodal information into a unified latent space.
- **MPMM**[Guo *et al.*, 2024]: A prompt-based multimodal framework that incorporates modality-aware prompts to stabilize learning under missing-modality settings. These prompts encode missingness patterns and guide the model toward more coherent multimodal representations.
- **MPLMM**[Lee *et al.*, 2023]: A lightweight Transformer architecture tailored for missing-modality scenarios. It integrates generation prompts, missing-signal prompts, and missing-type prompts to enhance cross-modal reasoning while keeping the number of trainable parameters low.

• **PMSM**[Liu *et al.*, 2025]: A prompt-matching sentiment analysis model targeting uncertain modality missingness. It employs unimodal prompt encoders for textual inputs and cross-modal prompts for audio and visual streams, connected via a bidirectional matching module with central-moment discrepancy losses. A comparator then synthesizes aligned missing features for final fusion.

• **CorrKD**[Li *et al.*, 2024]: A correlation-decoupled knowledge distillation framework in which a full-modality teacher delivers contrastive, prototype-based, and consistency distillation signals to a student model with missing modalities, improving semantic recovery and cross-modal robustness without relying on explicit reconstruction.

## D Additional Experimental Results

**Evaluation on Random Missing Modalities** To fully understand the capability of OMG-Agent in handling incomplete data, we performed a comprehensive evaluation on CMU-MOSI and CMU-MOSEI under various random missing rate settings. We set the Missing Rate (MR) to varying levels between 0.0 and 0.7. All models were trained and evaluated under aligned missing rates. The same MR was applied during both training and inference. The experiment results are reported in Table 2.

**Efficacy of Dual-Conditioning Injection** To validate the advantage of the “deep-semantics, shallow-details” strategy in preserving sentiment features, we compared our mechanism against three variants: (i) **Concat-Injection**, concatenating semantic vectors and evidence features for simultaneous injection into all layers; (ii) **Reversed-Injection**, injecting semantics into shallow layers and evidence into deep layers; and (iii) **Single-Stream**, only injecting evidence features into shallow layers. As shown in Table 4, Concat-Injection decreases ACC2 by 1.2%, and Reversed-Injection performs the worst. Deep analysis reveals that mixing features of different abstraction levels causes gradient interference, disrupting the structure of the Sentiment Manifold. Only our hierarchical design successfully decouples semantic intent from low-level signals, maximizing the discriminativeness of reconstructed features.

**Impact of Plan-Driven Retrieval Strategy** Regarding query construction in the retrieval module, we evaluated three settings: (i) **Content-Only**, using only observational features for retrieval; (ii) **Random-Plan**, fusing randomly sampled plan vectors; and (iii) **Plan-Driven**, fusing optimized semantic plans. As shown in Table 3, Experiments reveal that the Content-Only strategy tends to recall “signal-similar but sentiment-opposite” noise samples, getting a ACC2 drop of 5.2% and 4.6%. Random-Plan introduces further interference. Only incorporating correct plan constraints yields the highest ACC2, ensuring that retrieved evidence aligns with the target sentiment semantics.

## References

[Andrew *et al.*, 2013] Galen Andrew, Raman Arora, Jeff Bilmes, and Karen Livescu. Deep canonical correlation

Table 2: Performance comparison under different missing rates (MR from 0.0 to 0.7) on CMU-MOSI and CMU-MOSEI datasets. The ACC2 / F1 / ACC7 results are reported and the best results are highlighted in **bold**.

Dataset	Method	Missing Rate (MR)							
		0.0	0.1	0.2	0.3	0.4	0.5	0.6	0.7
CMU-MOSI	CCA	74.7 / 74.1 / 29.9	71.6 / 71.2 / 27.6	68.8 / 68.4 / 25.6	65.7 / 65.0 / 26.3	62.1 / 61.0 / 23.0	60.4 / 59.5 / 21.4	59.9 / 57.4 / 21.9	53.3 / 53.8 / 19.2
	AE	85.9 / 85.2 / 45.8	82.3 / 83.1 / 41.9	78.4 / 80.3 / 39.8	74.0 / 77.3 / 35.7	69.8 / 72.1 / 34.2	66.6 / 67.9 / 33.3	60.2 / 64.3 / 29.0	55.6 / 58.7 / 28.5
	DCCA	75.3 / 75.4 / 30.5	72.1 / 72.8 / 28.0	69.3 / 69.1 / 25.8	65.4 / 65.2 / 25.7	62.8 / 62.0 / 24.2	60.9 / 59.9 / 21.6	58.6 / 57.3 / 21.2	57.4 / 56.0 / 20.4
	DCCAE	77.3 / 77.4 / 31.2	74.5 / 74.7 / 28.1	71.8 / 71.9 / 27.6	67.0 / 66.7 / 25.8	63.6 / 62.8 / 24.2	62.0 / 61.3 / 23.0	59.6 / 58.5 / 20.9	58.1 / 57.4 / 20.6
	CRA	85.7 / 85.0 / 45.1	82.6 / 81.9 / 42.2	78.5 / 79.2 / 40.2	75.1 / 76.2 / 35.6	70.2 / 71.4 / 34.4	67.4 / 67.8 / 33.7	62.4 / 64.7 / 30.3	59.4 / 59.2 / 27.1
	MCTN	81.4 / 81.5 / 43.4	78.4 / 78.5 / 39.8	75.6 / 75.7 / 38.5	71.3 / 71.2 / 35.5	68.0 / 67.6 / 32.9	65.4 / 64.8 / 31.2	63.8 / 62.5 / 29.7	61.2 / 59.9 / 27.5
	MMIN	84.6 / 84.4 / 44.8	81.8 / 81.8 / 41.2	79.0 / 79.1 / 38.9	76.1 / 76.2 / 36.9	71.7 / 71.6 / 34.9	67.2 / 66.5 / 32.2	64.9 / 64.0 / 29.1	62.8 / 61.0 / 28.4
	TATE	83.3 / 83.0 / 44.7	83.2 / 82.6 / 42.4	80.8 / 81.7 / 38.6	79.9 / 80.6 / 36.5	77.8 / 79.3 / 34.7	73.0 / 73.7 / 32.7	68.3 / 64.1 / 31.1	61.9 / 62.4 / 28.8
	MPMM	83.2 / 83.8 / 43.2	81.0 / 80.8 / 41.3	79.0 / 78.9 / 39.7	77.5 / 77.2 / 38.9	76.0 / 74.8 / 38.0	74.0 / 74.0 / 37.5	73.2 / 73.4 / 36.8	71.3 / 71.9 / 35.6
	IMDer	85.7 / 85.6 / 45.3	84.8 / 84.8 / 44.8	83.5 / 83.4 / 44.3	81.2 / 81.0 / 42.5	78.6 / 78.1 / 39.7	76.2 / 75.9 / 37.9	74.7 / 74.0 / 35.8	71.9 / 71.2 / 33.4
	MPLMM	83.6 / 84.1 / 44.9	81.7 / 82.2 / 42.1	80.2 / 80.2 / 40.2	78.4 / 78.4 / 39.4	77.1 / 77.0 / 38.3	76.8 / 77.2 / 37.1	76.1 / 76.6 / 36.7	74.9 / 76.3 / 35.1
CMU-MOSEI	SMCSMA	85.8 / 86.1 / 39.2	85.1 / 85.4 / 38.0	83.6 / 83.3 / 37.5	81.4 / 81.1 / 36.3	79.7 / 79.3 / 35.3	77.4 / 77.5 / 33.7	75.0 / 73.5 / 27.6	72.2 / 71.5 / 28.0
	CorrKD	86.0 / 86.0 / 45.1	85.5 / 85.5 / 45.3	83.5 / 83.6 / 45.0	82.0 / 82.0 / 42.0	80.8 / 80.2 / 39.5	77.6 / 77.7 / 37.7	74.4 / 74.5 / 34.7	72.5 / 72.7 / 30.5
	PMMS	86.0 / 86.0 / 44.5	85.4 / 85.2 / 43.2	84.7 / 84.8 / 39.1	83.5 / 83.4 / 37.6	78.5 / 77.8 / 36.6	76.4 / 76.2 / 28.0	75.8 / 74.6 / 25.2	72.0 / 69.6 / 23.2
	<b>Ours</b>	<b>89.5 / 89.5 / 48.2</b>	<b>88.5 / 88.5 / 46.4</b>	<b>85.7 / 85.7 / 45.3</b>	<b>84.3 / 84.6 / 43.0</b>	<b>82.2 / 82.2 / 40.1</b>	<b>78.6 / 78.8 / 39.0</b>	<b>77.4 / 77.4 / 37.8</b>	<b>76.4 / 76.3 / 36.0</b>
	CCA	81.2 / 80.9 / 47.9	79.1 / 78.8 / 46.9	78.1 / 76.7 / 46.1	76.3 / 72.8 / 45.8	74.6 / 71.3 / 45.3	73.2 / 70.7 / 44.9	70.6 / 70.8 / 44.1	56.3 / 58.2 / 30.8
	AE	86.7 / 87.5 / 53.3	84.4 / 84.8 / 52.7	82.6 / 83.1 / 52.3	80.6 / 80.3 / 51.9	78.8 / 78.7 / 50.8	76.4 / 76.5 / 47.0	74.3 / 74.4 / 45.9	72.8 / 72.7 / 42.9
	DCCA	85.7 / 85.6 / 45.3	84.9 / 84.8 / 44.8	83.5 / 83.4 / 44.3	81.2 / 81.0 / 42.5	78.6 / 78.1 / 39.7	76.2 / 75.9 / 37.9	74.7 / 74.0 / 35.8	71.9 / 71.2 / 33.4
	DCCAE	81.2 / 81.2 / 48.2	78.4 / 78.3 / 46.9	75.5 / 75.4 / 46.3	72.3 / 72.2 / 45.6	70.3 / 70.0 / 44.0	69.2 / 66.4 / 43.3	67.6 / 63.2 / 42.9	66.6 / 62.6 / 42.5
	CRA	86.5 / 86.3 / 53.9	84.2 / 84.5 / 52.9	82.3 / 82.7 / 52.5	80.1 / 79.9 / 50.4	78.6 / 78.5 / 50.3	75.9 / 75.7 / 48.0	74.1 / 74.3 / 44.7	72.5 / 72.4 / 43.1
	MCTN	84.2 / 84.2 / 51.2	81.8 / 81.6 / 49.8	79.0 / 78.7 / 48.6	76.9 / 76.2 / 47.4	74.3 / 74.1 / 45.6	73.6 / 72.6 / 45.1	73.2 / 71.1 / 43.8	72.7 / 70.5 / 43.6
	MMIN	84.3 / 84.2 / 52.4	81.9 / 81.3 / 50.6	79.8 / 78.8 / 49.6	77.2 / 75.5 / 48.1	75.2 / 72.6 / 47.5	73.9 / 70.7 / 46.7	73.2 / 70.3 / 45.6	73.1 / 69.5 / 44.8
	TATE	82.9 / 84.1 / 50.1	83.4 / 83.9 / 49.8	81.8 / 81.1 / 49.4	80.4 / 79.5 / 48.8	78.1 / 77.8 / 47.8	75.7 / 75.6 / 45.1	68.5 / 64.6 / 33.0	62.3 / 62.9 / 30.2
	MPMTM	83.8 / 82.5 / 47.6	79.0 / 79.5 / 46.7	78.1 / 77.3 / 45.9	76.7 / 75.3 / 47.7	74.3 / 73.9 / 43.1	73.6 / 73.5 / 42.1	72.6 / 72.4 / 35.8	72.4 / 71.5 / 33.7
	IMDer	85.1 / 85.1 / 53.4	84.8 / 84.6 / 53.1	82.7 / 82.4 / 52.0	81.3 / 80.7 / 51.3	79.3 / 78.1 / 50.0	79.0 / 77.4 / 49.2	78.0 / 75.5 / 48.5	77.3 / 74.6 / 47.6
	MPLMM	85.1 / 84.5 / 53.6	83.5 / 82.8 / 51.5	82.1 / 81.6 / 48.7	78.5 / 78.8 / 46.8	77.6 / 77.6 / 45.7	76.6 / 76.7 / 44.8	75.4 / 75.6 / 43.0	74.3 / 74.1 / 42.2
	SMCSMA	80.6 / 80.9 / 50.7	79.0 / 79.3 / 50.4	77.0 / 77.3 / 50.3	76.2 / 76.5 / 50.0	74.5 / 74.7 / 49.2	72.1 / 72.2 / 49.1	71.2 / 71.2 / 48.7	70.3 / 70.4 / 48.0
	CorrKD	85.7 / 85.6 / 52.0	84.2 / 84.2 / 51.6	82.6 / 82.7 / 51.4	80.8 / 80.8 / 49.8	79.5 / 79.3 / 49.1	77.0 / 76.1 / 47.9	76.6 / 76.5 / 47.8	76.0 / 75.7 / 47.5
	PMMS	85.1 / 84.8 / 53.4	84.0 / 83.9 / 51.7	82.5 / 82.5 / 49.2	80.8 / 80.8 / 48.2	79.4 / 79.6 / 47.9	77.8 / 78.1 / 47.3	76.5 / 77.0 / 43.3	72.0 / 72.7 / 40.7
	<b>Ours</b>	<b>87.6 / 87.8 / 56.7</b>	<b>86.4 / 86.5 / 55.4</b>	<b>85.0 / 85.0 / 54.5</b>	<b>82.8 / 82.6 / 53.9</b>	<b>80.5 / 80.5 / 52.5</b>	<b>79.2 / 78.7 / 51.0</b>	<b>78.4 / 77.7 / 50.3</b>	<b>77.4 / 75.0 / 48.5</b>

Table 3: Ablation study of the Plan-Driven Retrieval Strategy on CMU-MOSI and CMU-MOSEI. The best ACC2 / F1 / ACC7 results are highlighted in **bold**.

Retrieval Strategy	CMU-MOSI	CMU-MOSEI
Content-Only Retrieval	74.4 / 72.1 / 32.5	74.0 / 73.8 / 46.6
Random-Plan Retrieval	71.2 / 71.0 / 26.7	72.8 / 73.4 / 43.2
<b>Plan-Driven Retrieval (Ours)</b>	<b>76.4 / 76.3 / 36.0</b>	<b>77.4 / 75.0 / 48.5</b>

Table 4: Ablation study of Dual-Conditioning Injection on CMU-MOSI and CMU-MOSEI. The best ACC2 / F1 / ACC7 results are highlighted in **bold**.

Variants	CMU-MOSI	CMU-MOSEI
<b>Ours</b>	<b>76.4 / 76.3 / 36.0</b>	<b>77.4 / 75.0 / 48.5</b>
Concat-Injection	75.2 / 74.6 / 34.8	76.2 / 73.6 / 46.4
Reversed-Injection	70.2 / 71.0 / 29.6	71.5 / 72.2 / 43.3
Single-Stream	73.2 / 73.2 / 31.8	75.3 / 74.5 / 45.8

analysis. In *International conference on machine learning*, pages 1247–1255. PMLR, 2013.

[Guo *et al.*, 2024] Zirun Guo, Tao Jin, and Zhou Zhao. Multimodal prompt learning with missing modalities for sentiment analysis and emotion recognition. *arXiv preprint arXiv:2407.05374*, 2024.

[Hinton and Salakhutdinov, 2006] Geoffrey E Hinton and Ruslan R Salakhutdinov. Reducing the dimensionality of data with neural networks. *science*, 313(5786):504–507, 2006.

[Hotelling, 1992] Harold Hotelling. Relations between two

sets of variates. In *Breakthroughs in statistics: methodology and distribution*, pages 162–190. Springer, 1992.

[Lee *et al.*, 2023] Yi-Lun Lee, Yi-Hsuan Tsai, Wei-Chen Chiu, and Chen-Yu Lee. Multimodal prompting with missing modalities for visual recognition. In *Proceedings of the IEEE/CVF Conference on Computer Vision and Pattern Recognition*, pages 14943–14952, 2023.

[Li *et al.*, 2024] Mingcheng Li, Dingkang Yang, Xiao Zhao, Shuaibing Wang, Yan Wang, Kun Yang, Mingyang Sun, Dongliang Kou, Ziyun Qian, and Lihua Zhang. Correlation-decoupled knowledge distillation for multimodal sentiment analysis with incomplete modalities. In *Proceedings of the IEEE/CVF Conference on Computer Vision and Pattern Recognition*, pages 12458–12468, 2024.

[Liu *et al.*, 2025] Jiaqi Liu, Yong Wang, Jing Yang, Fanshu Shang, and Fan He. Prompt-matching synthesis model for missing modalities in sentiment analysis. *Knowledge-Based Systems*, page 113519, 2025.

[Pham *et al.*, 2019] Hai Pham, Paul Pu Liang, Thomas Manzini, Louis-Philippe Morency, and Barnabás Póczos. Found in translation: Learning robust joint representations by cyclic translations between modalities. In *Proceedings of the AAAI conference on artificial intelligence*, volume 33, pages 6892–6899, 2019.

[Sun *et al.*, 2024] Yuhang Sun, Zhizhong Liu, Quan Z Sheng, Dianhui Chu, Jian Yu, and Hongxiang Sun. Similar modality completion-based multimodal sentiment analysis under uncertain missing modalities. *Information Fusion*, 110:102454, 2024.

[Tran *et al.*, 2017] Luan Tran, Xiaoming Liu, Jiayu Zhou, and Rong Jin. Missing modalities imputation via cascaded residual autoencoder. In *Proceedings of the IEEE conference on computer vision and pattern recognition*, pages 1405–1414, 2017.

[Wang *et al.*, 2015] Weiran Wang, Raman Arora, Karen Livescu, and Jeff Bilmes. On deep multi-view representation learning. In *International conference on machine learning*, pages 1083–1092. PMLR, 2015.

[Wang *et al.*, 2023a] Yuanzhi Wang, Zhen Cui, and Yong Li. Distribution-consistent modal recovering for incomplete multimodal learning. In *Proceedings of the IEEE/CVF International Conference on Computer Vision*, pages 22025–22034, 2023.

[Wang *et al.*, 2023b] Yuanzhi Wang, Yong Li, and Zhen Cui. Incomplete multimodality-diffused emotion recognition. *Advances in Neural Information Processing Systems*, 36:17117–17128, 2023.

[Yu *et al.*, 2020] Wenmeng Yu, Hua Xu, Fanyang Meng, Yilin Zhu, Yixiao Ma, Jiele Wu, Jiyun Zou, and Kaicheng Yang. Ch-sims: A chinese multimodal sentiment analysis dataset with fine-grained annotation of modality. In *Proceedings of the 58th annual meeting of the association for computational linguistics*, pages 3718–3727, 2020.

[Zadeh *et al.*, 2016] Amir Zadeh, Rowan Zellers, Eli Pincus, and Louis-Philippe Morency. Mosi: multimodal corpus of sentiment intensity and subjectivity analysis in online opinion videos. *arXiv preprint arXiv:1606.06259*, 2016.

[Zadeh *et al.*, 2018] AmirAli Bagher Zadeh, Paul Pu Liang, Soujanya Poria, Erik Cambria, and Louis-Philippe Morency. Multimodal language analysis in the wild: Cmu-mosei dataset and interpretable dynamic fusion graph. In *Proceedings of the 56th Annual Meeting of the Association for Computational Linguistics (Volume 1: Long Papers)*, pages 2236–2246, 2018.

[Zeng *et al.*, 2022] Jiandian Zeng, Tianyi Liu, and Jiantao Zhou. Tag-assisted multimodal sentiment analysis under uncertain missing modalities. In *Proceedings of the 45th International ACM SIGIR Conference on Research and Development in Information Retrieval*, pages 1545–1554, 2022.

[Zhao *et al.*, 2021] Jinming Zhao, Ruichen Li, and Qin Jin. Missing modality imagination network for emotion recognition with uncertain missing modalities. In *Proceedings of the 59th Annual Meeting of the Association for Computational Linguistics and the 11th International Joint Conference on Natural Language Processing (Volume 1: Long Papers)*, pages 2608–2618, 2021.